PCCP

Relevance of hydrogen bonded associates on the transport properties and nanoscale dynamics of liquid and supercooled 2-propanol

Journal:	*Physical Chemistry Chemical Physics*
Manuscript ID	CP-ART-10-2020-005481.R2
Article Type:	Paper
Date Submitted by the Author:	01-Mar-2021

Complete List of Authors:	Zhai, Yanqin; University of Illinois at Urbana-Champaign, Luo, Peng; UIUC, Beckman Institute for Advanced Science and Technology Nagao, Michihiro; NIST, NCNR; Indiana University, CEEM Nakajima, Kenji; Japan Atomic Energy Agency Kikuchi, Tatsuya; Japan Atomic Energy Agency Kawakita, Yukinobu; Japan Atomic Energy Agency Kienzle, Paul; National Institute of Standards and Technology, NIST Center for Neutron Research Z, Y; University of Illinois at Urbana-Champaign, Nuclear, Plasma, and Radiological Engineering, Department of Materials Science and Engineering, Department of Electrical and Computer Engineering Faraone, Antonio; NIST,

PCCP

ARTICLE TYPE

Cite this: DOI: 00.0000/xxxxxxxxxx

Relevance of hydrogen bonded associates on the transport properties and nanoscale dynamics of liquid and supercooled 2-propanol†

Yanqin Zhai,[ab] Peng Luo,[b] Michihiro Nagao[cde], Kenji Nakajima[f], Tatsuya Kikuchi[f], Yukinobu Kawakita[f], Paul A. Kienzle[c], Y Z*[abg], and Antonio Faraone*[c]

Received Date
Accepted Date

DOI: 00.0000/xxxxxxxxxx

2-propanol was investigated, in both the liquid and supercooled states, as a model system to study how hydrogen bonds affect the structural relaxation and the dynamics of mesoscale structures, of approximately several Ångstroms, employing static and quasi-elastic neutron scattering and molecular dynamics simulation. Dynamic neutron scattering measurements were performed over an exchanged wave-vector range encompassing the pre-peak, indicative of the presence of H-bonding associates, and the main peak. The dynamics observed at the pre-peak is associated with the formation and disaggregation of the H-bonded associates and is measured to be at least one order of magnitude slower than the dynamics at the main peak, which is identified as the structural relaxation. The measurements indicate that the macroscopic shear viscosity has a similar temperature dependence as the dynamics of the H-bonded associates, which highlights the important role played by these structures, together with the structural relaxation, in defining the macroscopic rheological properties of the system. Importantly, the characteristic relaxation time at the pre-peak follows an Arrhenius temperature dependence whereas at the main peak exhibits a non-Arrhenius behavior on approaching the supercooled state. The origin of this differing behavior is attributed to an increased structuring of the hydrophobic domains of 2-propanol accommodating a more and more encompassing H-bond network, and a consequent set in of dynamic cooperativity.

1 Introduction

Through the formation of hydrogen bonds, hydroxyl groups play a significant role in affecting the interactions between molecules including both small molecular liquids such as water[1–6] and macromolecular assemblies such as deoxyribonucleic acids[7–9] and proteins[10–13]. As one of the simplest type of model system to study the effect of hydrogen bonding on the structure and dynamics of molecular liquids, monohydroxy alcohols have attracted research interest for decades[14–26].

Hydrogen bonding can lead to the formation of supramolecular clusters and introduce mesoscale structuring typically characterized by a structure factor pre-peak at smaller Q values than the main peak, Q being the exchanged wavevector in scattering experiments[17,18,25,27]. The shapes of the clusters formed by hydrogen bonding are usually believed to be chains, trees, or rings[28–39] and can vary according to the position of the hydroxyl group.

The fundamental relaxation process or structural relaxation in liquids is a measure of the time scale of molecular rearrangements. It can be probed by dielectric or mechanical relaxation spectroscopy[40–43], typically referred to as the α-relaxation, as well as by scattering measurements at the main peak[21–23,44,45]. In addition to the α-relaxation, Debye first observed in the dielectric response of monohydroxy alcohols[46] the existence of an additional prominent, Lorentzian, slow relaxation process, nowadays most commonly referred to as the Debye process, which is still object of active research[47]. Recent studies suggested that in monohydroxy alcohols the α-relaxation originates from the motion of the alkyl chains, whereas the Debye process is related to the dynamics of the supramolecular clusters formed by hydrogen bonding[19,21]. Other relaxation processes have also been observed such as the Johari-Goldstein relaxation[48,49].

Neutron scattering techniques are able to probe structures from sub-Å to micrometers and dynamics from sub-picoseconds

[a] Department of Nuclear, Plasma, and Radiological Engineering, University of Illinois at Urbana-Champaign, Urbana, Illinois 61801, USA
[b] Beckman Institute for Advanced Science and Technology, University of Illinois at Urbana-Champaign, Urbana, Illinois 61801, USA
[c] NIST Center for Neutron Research, National Institute of Standards and Technology, Gaithersburg, Maryland 20899, USA
[d] Center for Exploration of Energy and Matter, Indiana University, Bloomington, Indiana 47408, USA
[e] Department of Physics and Astronomy, University of Delaware, Newark, Delaware 19716, USA
[f] J-PARC Center, Japan Atomic Energy Agency, Tokai, Ibaraki 319-1195, Japan
[g] Department of Electrical and Computer Engineering, University of Illinois at Urbana-Champaign, Urbana, Illinois 61801, USA
† Electronic Supplementary Information (ESI) available: Attached after the main text. See DOI: 10.1039/cXCP00000x/

to nearly microseconds, which covers the relevant length scale and time scale of relaxation of monohydroxy alcohols. For example, neutron Time-of-Flight (ToF)[50] and Spin-Echo (NSE)[51] spectroscopy, combined with dielectric and near-infrared spectroscopy, have been employed to study the connection between structure and dynamics in 1-propanol by Sillrén *et al.*[21]. As a complement to neutron scattering experiments, molecular dynamics (MD) simulation is useful to reveal the underlying mechanisms of the dynamics of interest. In the past, a number of neutron scattering studies in conjunction with MD simulations have been performed on the dynamics of mesoscale structures in mono hydroxyalcohols such as methanol[22–24] and dodecanol[26] in the liquid state.

Of particular interest in glass-forming liquids are the onset of a (often super-Arrhenius) dynamical slowing down, the transition of dynamics from uncorrelated to correlated, the emergence of dynamical heterogeneity, as well as the breakdown of the Stokes-Einstein relation. The origin of these phenomena is a fundamental unsolved problem in condensed matter physics. Whether it is related to any structural correlation is still under debate. It has been shown that the glass transition could be associated with specific structural organization, which, however, cannot typically be probed by conventional experimental techniques but can be accessed by computer simulations[52,53]. Therefore, a systematic study of the dynamics of H-bonded associated structures in monohydroxy alcohols is not only crucial to link their microscopic and macroscopic properties, but also relevant, when extended to the supercooled state, to the understanding of glassy phenomena. However, simple monohydroxy alcohols have a propensity to crystallize and thus previous neutron spectroscopy studies have not investigated the supercooled state.

2-propanol (melting temperature $T_m = 184$ K, glass transition temperature $T_g = 118.8$ K[15]), as the simplest monohydroxy alcohol with the hydroxyl group located in a non-terminal position, together with its important applications in the chemical industry, is regarded as an interesting model system for studying the correlation between structure and dynamics of hydrogen bonded liquids. The non-terminal position of the hydroxyl group endows it with different characteristics than 1-propanol. For example, it has been shown that the breakage of the hydrogen bond network needs to occur for crystallization to take place in 2-propanol.[54] Whereas, 1-propanol is believed to form H-bonded associates overwhelmingly in the form of chains, it has been suggested that 2-propanol molecules form ring structures.[17] In this work, we performed static and Quasi-Elastic Neutron Scattering (QENS) experiments[55] and MD simulations to study the connection between the structure and dynamics in 2-propanol in the liquid and supercooled state. Using a QENS ToF and an NSE spectrometer, we covered a time range from a few picoseconds to tens of nanoseconds. Moreover, NSE spectrometers, as detailed in the methods section, measure scattering in which the collective dynamics contribution, relevant to the structural and mesoscale relaxation, is enhanced compared to other neutron spectrometers. By analyzing the neutron scattering experimental results, we found that the dynamics at the structure factor pre-peak is at least one order of magnitude slower than at the main peak. We interpret this observation as a consequence of the emergence of supramolecular clusters associated by hydrogen bonds. The similarity of the activation energies for the viscosity and for the dynamics at the pre-peak indicates that the dynamics of the clusters significantly contributes, together with the structural relaxation, to the macroscopic rheological properties. Furthermore, for the first time, we report of a case for which the temperature dependence of the dynamics is different at the structure factor pre-peak and main peak. Our finding provides fundamental experimental insights for understanding the connection between the meso-scale structure, dynamics and macroscopic rheological properties in associated liquids.

2 Method

2.1 Neutron scattering experiment

2.1.1 Theory

Dynamic scattering measurements determine the dynamics structure factor $S(Q,E)$. For Quasi-Elastic Neutron Scattering (QENS), the measured scattering intensity is constituted of the coherent dynamic structure factor, $S_{\mathrm{coh}}(Q,E)$, which depends on the correlation between the positions of the same and different nuclei at different times and the incoherent term, $S_{\mathrm{inc}}(Q,E)$, which depends only on the correlation between the positions of the same nucleus at different times[56]. Thus, it can be expressed as

$$S(Q,E) = S_{\mathrm{coh}}(Q,E) + S_{\mathrm{inc}}(Q,E) \tag{1}$$

The coherent dynamic structure factor is the Fourier transform of the collective Intermediate Scattering Function (ISF) as[57]

$$S_{\mathrm{coh}}(Q,E) = \frac{1}{2\pi\hbar}\int_{-\infty}^{\infty} F_{\mathrm{c}}(Q,t)e^{-i\frac{E}{\hbar}t}dt \tag{2}$$

where the collective ISF is defined as

$$F_{\mathrm{c}}(Q,t) = \frac{1}{N\langle b^{\mathrm{coh}}\rangle^2}\left\langle \sum_{l=1}^{N}\sum_{l'=1}^{N} b_l^{\mathrm{coh}} b_{l'}^{\mathrm{coh}} e^{iQ\cdot[R_l(t)-R_{l'}(0)]}\right\rangle \tag{3}$$

In Equation 3, N is the number of atoms in the system, b_l^{coh} and $R_l(t)$ represent, the coherent neutron scattering length, and the position at time t, of the l-th atom, and $\langle\cdots\rangle$ indicates an ensemble average.

Similarly, the incoherent dynamic structure factor is defined as the Fourier transform of the single particle (self) ISF[57],

$$S_{\mathrm{inc}}(Q,E) = \frac{1}{2\pi\hbar}\int_{-\infty}^{\infty} F_{\mathrm{s}}(Q,t)e^{-i\frac{E}{\hbar}t}dt \tag{4}$$

where

$$F_{\mathrm{s}}(Q,t) = \frac{1}{N\langle (b^{\mathrm{inc}})^2\rangle}\left\langle \sum_{l=1}^{N} (b_l^{\mathrm{inc}})^2 e^{iQ\cdot[R_l(t)-R_l(0)]}\right\rangle \tag{5}$$

In Equation 5, b_l^{inc} represents the incoherent neutron scattering length of the l-th atom.

Different from conventional neutron scattering techniques, NSE spectrometers directly measure the normalized ISF. In NSE, the dynamic information is encoded into the spins of the neutrons; since incoherent scattering has a 1/3 probability of flipping

the spin direction, the normalized ISF measured by NSE is[51,58]

$$I^{\mathrm{NSE}} = \frac{F_{\mathrm{c}}(Q,t) - \frac{1}{3}F_{\mathrm{s}}(Q,t)}{F_{\mathrm{c}}(Q,0) - \frac{1}{3}F_{\mathrm{s}}(Q,0)} \quad (6)$$

In a neutron diffraction measurement, as no energy analysis is carried out, the measured quantity is (within a certain approximation) the static structure factor:

$$S(Q) = \int_{-\infty}^{\infty} S(Q,E)\mathrm{d}E \quad (7)$$

The structure factor provides information on the instantaneous correlation between atoms' positions. In addition, polarized neutron diffraction measurements can be performed on NSE, enabling the separation of the coherent and incoherent contributions[59].

2.1.2 Experiment details

Three different fully and partially deuterated 2-propanol and one fully deuterated 1-propanol samples were prepared. The fully deuterated 2-propanol (CD_3-CDOD-CD_3, 99%-D) was purchased from Cambridge Isotope Laboratories, Inc. The propyl partially deuterated (CD_3-CDOH-CD_3, 99.7%-D) and hydroxyl partially deuterated (CH_3-CHOD-CH_3, 98%-D) 2-propanol samples were purchased from CDN Isotopes. Fully deuterated 1-propanol (CD_3-CD_2-CD_2OD, 99.1%-D) was purchased from CDN Isotopes. All the samples were used as received. Samples were contained in aluminum cans sealed with indium in an annular geometry.

The QENS and NSE measurements on 2-propanol were performed between 280 K and 120 K. Temperature was controlled using a closed cycle refrigerator with an accuracy better than 1 K. Because of the propensity for crystallization below its melting point (184 K), to investigate the supercooled state temperature was continually cycled between 200 K and 120 K, at 1 K/min, while data were collected in batches of 4 mins. The structure after each cycle was checked to verify the absence of crystallization; however, because of the way the measurements were acquired and the lack of equilibration time, the actual temperature of the sample lagged behind (it was higher) than the one recorded by the temperature control system. The temperature offset was determined by comparing the data measured in the range between 200 K and 180 K for which data at temperature equilibrium were acquired. As detailed in Figure S7[60] the nominal *vs* actual temperature difference was determined to be negligible for the measurements at the main peak and ≈6 K at the pre-peak, owing to the fact that this latter measurements were performed with double the amount of sample to compensate for the lack of scattering intensity. Temperature uncertainty was set at ±2 K to account for these effects and for the fact that the measurements were taken while the temperature was changing.

Polarized neutron diffraction and NSE measurements were carried out at the National Institute of Standards and Technology (NIST) Center for Neutron Research (NCNR)[58], whereas the QENS measurements were performed on the Time-of-Flight (ToF) spectrometer AMATERAS at J-PARC in Japan[61].

Polarized neutron diffraction measurements on fully and partially deuterated 2-propanol as well as on deuterated 1-propanol were performed using 5 Å incoming neutrons with $\Delta\lambda/\lambda \approx 20\%$. The empty can contribution was subtracted after correction for self-shielding approximated by the transmission.

For the NSE measurements, the incoming wavelength of neutrons was set to 5 Å or 6 Å with $\Delta\lambda/\lambda \approx 20\%$. The dynamic range probed extended from several picoseconds up to 20 nanoseconds. Data were collected in correspondence to the pre-peak at 0.8 $\mathrm{Å}^{-1}$ and the main peak at 1.45 $\mathrm{Å}^{-1}$. The instrumental energy resolution was measured using a standard $Ti_{2.08}Zr$ sample. Data were reduced to normalized ISFs using the Data Analysis and Visualization Environment (DAVE) software[62].

The QENS measurements were performed using multi-E_i technique[63] where spectra for three configurations of incident neutron energy of (1.7, 3,1 and 7.7) meV were simultaneously measured. The corresponding instrumental energy resolutions approximate Gaussian functions with Full Width at Half Maximum (FWHM) of about (10, 30 and 100) μeV, respectively. To determine the detector efficiencies and the instrumental energy resolution, a standard vanadium sample and the scattering from the same sample in the vitreous state at 10 K, respectively, were measured. Data were corrected for the scattering from the empty can and reduced to constant Q spectra using the software Utsusemi and M-slice[62,64].

2.1.3 Data analysis

QENS data measured were fitted by a curve fitting and uncertainty analysis software—Bumps[65] which allowed for a global fit of the data from the three configurations employed. Bumps casts curve fitting as a Bayesian optimization problem with the goal of determining the probability of observing parameter values M given the measured data D, which is written as P(M|D). This is related by Bayes Rule to P(D|M), the probability of observing D given M and P(M), the prior probability on the parameters, with $P(M|D) \propto P(D|M)P(M)$. Using Markov chain Monte Carlo (MCMC) with adaptive stepping (DREAM[66]), Bumps samples from the posterior probability P(M|D), from which we can estimate mean, standard deviation, Bayesian credible intervals, maximum likelihood, and correlations between model parameters. The sampling process is robust, allowing Bumps to step out of local minima and eventually find the global minimum. At each temperature and wavevector, the data measured with different instrumental resolutions were fitted with a same set of parameters. Therefore, the fitting results are the global fits suitable for all instrumental resolutions.

With respect to the QENS data, the analysis of the NSE data is computationally much simpler as it does not require numerical convolution and Fourier transform (as detailed in the following Equations 8, 9, and 10). The data were analyzed using least square minimization routines available in MATLAB[67]. These routines were also used to perform global fitting of the NSE data for the same Q value at various temperatures.

2.2 Viscosity measurement

Viscosity measurements on fully deuterated 2-propanol were conducted using an Anton Paar MCR 501 stress-controlled rheometer. A titanium Mooney-Ewart concentric cylinder was employed,

with an inner cylinder radius of 28.0 mm and a gap between the inner and outer cylinders of 1.0 mm. The geometry was used as specified by the manufacturer and appropriate steps were taken to minimize measurement artifacts and correct for system inertia.

2.3 Molecular dynamics simulation

In this work, MD simulations were carried out to study the microscopic structure and dynamics of 2-propanol using GROMACS 5.0.7[68]. 2000 hydrogenated 2-propanol molecules were placed in a cubic simulation box with periodic boundary conditions enforced in all directions. OPLS-AA force field[69] was employed to describe the interaction between 2-propanol molecules. Chemical bonds involved in hydrogen atoms were constrained using LINCS algorithm[70]. The Lennard-Jones interactions were truncated at 1.0 nm and the electrostatic interaction was computed by the particle-mesh Ewald method[71] with a real-space cutoff of 1.0 nm. The simulations were performed in the *NPT* ensemble using a Nosé-Hoover thermostat[72–74] and a Parrinello-Rahman barostat[75,76] with an integration time step of 1 fs using a leap-frog integrator. At each condition, the system was equilibrated for 10 ns and the trajectory was collected in the following 15 ns. In the coherent structure factor $S_{\mathrm{coh}}(Q)$, the interval of Q is limited by the box length. In order to obtain a higher Q-resolution during the computation of structure factor, we created larger simulation boxes with doubled side length with 16000 2-propanol molecules inside at each target temperature. The preparation and data collection of the systems followed the same procedure described above. Hydrogen bond analysis was performed using the *hbond* package of GROMACS. Other static and dynamic quantities were calculated using *LiquidLib*[77]. All hydrogen atoms were simulated as ^{1}H during the simulations, whereas part of them were weighted using the scattering length of deuterium while calculating the static and dynamic quantities in order to compare with the experimental results. A comparison between simulated density and experimental values as a function of temperature is shown in Figure S1[60].

3 Results and Discussion

3.1 Structure

A structure factor pre-peak at $Q \approx 0.75$ Å^{-1} together with the main peak at $Q = 1.45$ Å^{-1} are identified by both polarized neutron diffraction measurements and MD simulations at $T = 280$ K, as shown in Figure 1. These observations are consistent with previous diffraction experiments[14,18]. The main peak at $Q = 1.45$ Å^{-1} corresponds to a distance of $2\pi/(1.45$ Å$^{-1}) \approx 4.3$ Å in real space which approximately matches the average distance between 2-propanol molecules. Fully and hydroxyl partially deuterated samples show obvious pre-peaks whereas the propyl partially deuterated sample does not. The partial structure factor calculated from MD trajectories involving atoms of propyl groups does not show an evident pre-peak; however, that involving only atoms of hydroxyl groups shows a strong feature in correspondence to the pre-peak. Both experimental and simulation results indicate the origin of the pre-peak to be the correlation between the hydroxyl groups. The picture that the pre-peak originates from the

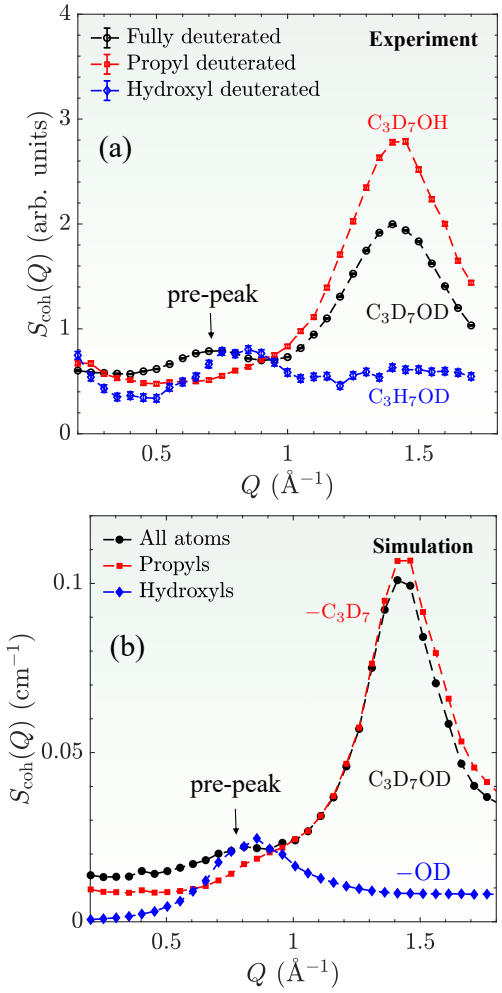

Fig. 1 (a) Coherent structure factors of fully, propyl partially, and hydroxyl partially deuterated 2-propanol at 280 K measured by polarized neutron diffraction experiments. The fully and hydroxyl partially deuterated samples show an obvious pre-peak at $Q \approx 0.75$ Å^{-1} whereas the propyl partially deuterated sample does not show the pre-peak around the corresponding Q range. The low Q upturn is an artifact due to the instrumental background. (b) Coherent all-atom and partial structure factors of fully deuterated 2-propanol at 280 K calculated from MD simulations using *LiquidLib*[77]. The structure factors are normalized by the volume of the system and thus has the unit of cm^{-1}. The all-atom coherent structure factor successfully reproduces the structure factor pre-peak observed in experiments. The partial structure factor of atoms in propyl groups does not show an evident pre-peak; however, the partial structure factor of atoms in hydroxyl groups shows a strong peak in correspondence to the pre-peak.

Table 1 Fractions of particles associated with different number of hydrogen bonds at temperatures ranging from 200 K to 280 K

	0 H-bond	1 H-bond	2 H-bonds	3 H-bonds
200 K	0.0016	0.0696	0.8699	0.0584
220 K	0.0025	0.0699	0.8765	0.0506
240 K	0.0045	0.0876	0.8553	0.0520
260 K	0.0078	0.1143	0.8237	0.0537
280 K	0.0149	0.1510	0.7811	0.0525

correlation between hydroxyl groups agrees with the common understanding that the pre-peak position is related to the average distance between adjacent supramolecular clusters formed by hydrogen bonding[21,23,26,78]. Recent simulation work also suggests that the pre-peak results from the aggregation of alcohol molecular clusters which introduces long-range correlation[79].

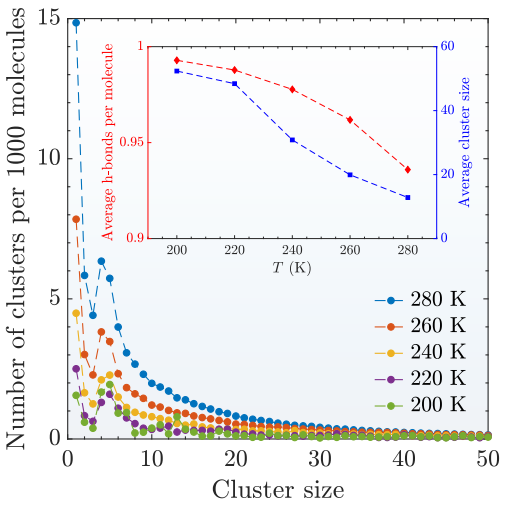

Fig. 2 Size distributions of the supramolecular clusters formed by hydrogen bonding at temperatures ranging from 280 K to 200 K. The inset shows the average number of hydrogen bonds per molecule and the average number of molecules per cluster size as functions of temperature. The number of molecules per cluster is defined as the number of 2-propanol molecules connected by hydrogen bonds within the same supramolecular cluster. The average H-bonds per molecule is defined as the total number of H-bonds formed between molecules divided by the total number of molecules. This figure only presents the cluster size distribution below 50 for visualization purpose. The distribution between 50 to 1000 is presented in Figure S2[60].

To understand the structure of 2-propanol in detail, we analyzed the supramolecular clusters formed by hydrogen bonding from the MD trajectories. The criterion for the existence of a hydrogen bond is when the distance between the donor and acceptor oxygen is less than 3.5 Å and the hydrogen-donor-acceptor angle is less than 30°[80].

Figure 2 shows the size distribution of the supramolecular clusters (see also Figure S2[60]), with the inset showing the average number of hydrogen bonds per molecule and the average cluster size. Among all measured temperatures, the average number of hydrogen bonds per molecule changes less than 7%, nevertheless, the constitution of clusters varies drastically. To be specific,

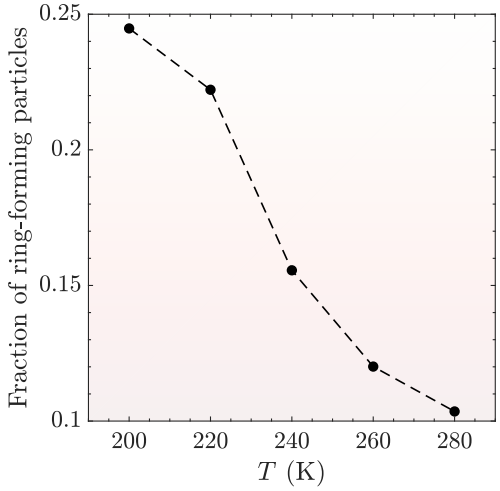

Fig. 3 Fractions of particles forming ring-like structures at temperatures ranging from 200 K to 280 K. This quantity is obtained by identifying all the ring-structures in the system and dividing the number of ring-forming particles by the total number of particles, which then is averaged over frames.

2-propanol molecules are prone to forming clusters with smaller sizes at higher temperature, for example, ≈ 15 molecules at 280 K. However, as temperature decreases, the average size of the clusters increases noticeably and the number of large cluster becomes increasingly significant. Nevertheless, forming clusters involving 4 or 5 molecules is preferred at all accessed temperatures, which is consistent with previous simulation on similar monohydroxy alcohols[81].

Further analysis of the MD data, shown in Table 1, also indicates that most molecules form two H-bonds and this fraction increases with decreasing temperature. Note that the average H-bonds per molecules in this case is close to 1 in Figure 2, since each H-bond connects two molecules, and thus, it only contributes 0.5 to the average value per molecule. These molecules are in the middle of either chain or ring structures. Molecules forming one H-bond only are at the end of chain- or tree-like structures. A very small fraction of molecules is not involved in H-bond at all, whereas a small but non-negligible percentage of about 5 % of molecules forms three H-bonds indicating the existence of branching and tree structures. Moreover, as temperature decreases, the fraction of molecules involved in two H-bonds increases at the expense of the one involved in only one H-bond; this finding is also reflected by the increase of the fraction of molecules forming ring-like associates as shown in Figure 3. Such fraction reaches almost 25 % at 200 K. *

These findings cannot be verified easily even with refined spectroscopic techniques, however, we are confident in the main result

* The ring-like structures are characterized by a Depth-First Search (DFS) algorithm. The snapshots of the MD trajectories are regarded as undirected graphs with molecules being vertices and H-bonds being edges. The ring-like structures are defined as the loops in the undirected graph. A molecule is defined as a ring-forming molecule if it is contained by any ring-like structure.

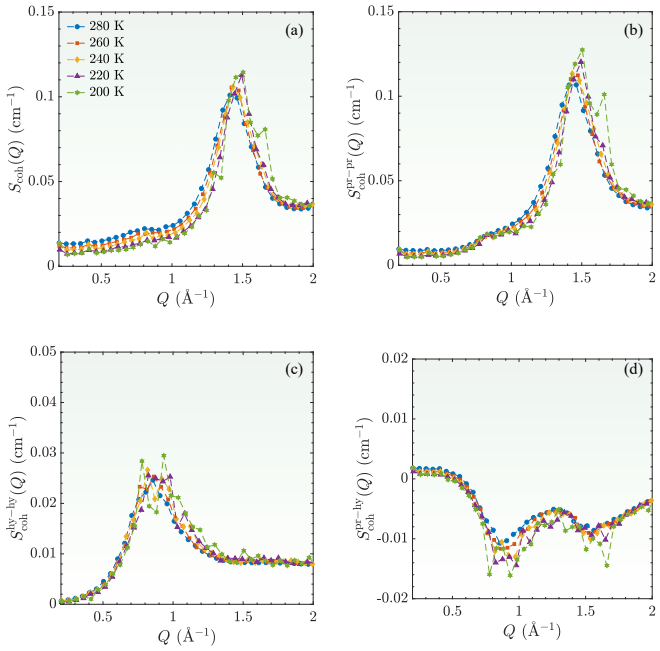

Fig. 4 Coherent (a) all atoms, (b) iso-propyl groups, (c) hydroxyl groups, and (d) cross term between propyl and hydroxyl groups structure factor of deuterated 2-propanol from 200 K to 280 K calculated from MD simulations.

that the extent of the hydrogen bond network increases with lowering the temperature. On the other hand, Zetterström *et al.* have reported that the intensity of the pre-peak decreases with temperature without speculating its origin[14]. This occurrence was also observed by us using polarized neutron diffraction as shown in Figure S3[60]. Incidentally, the same temperature dependence on the intensity of the structure factor pre-peak is also observed in 1-propanol (see Figure S4[60]), which suggests the non-terminal position of the hydroxyl group is not connected with the origin of this behavior. The apparently contradicting indications of an increase of H-bonding association and decrease of pre-peak intensity can be explained considering the partial components of the structure factor. As mentioned above, at room temperature the pre-peak mainly originates from the partial structure factors of the atoms of the hydroxyl group, whereas the other atoms are responsible for the main peak. The cross term is actually negative with a valley roughly in correspondence of the pre-peak; this term is negative because of the anticorrelation between the position of the hydroxyl and propyl groups in 2-propanol, due to hydrogen bonding association. Partial isotopic substitution changes the sign of the cross-term partial structure factor because the coherent scattering length of H and D have opposite sign and the pre-peak is therefore enhanced, as shown in Figure 1. As temperature is lowered, the ordering of the propyl groups with respect to the hydroxyl groups of 2-propanol increases, matching the motif imposed by the hydrogen bond network. Partial structure factors calculated from the MD trajectories reported in Figure 4 supports this hypothesis. To further support this scenario, we report in Figure 5 the integrated spectral scattering intensity measured on AM-

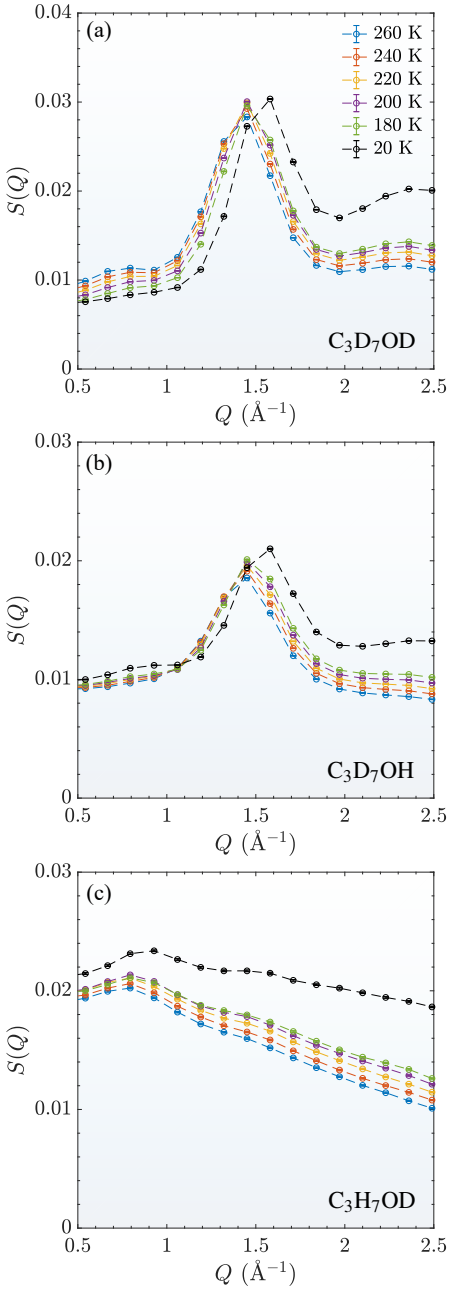

Fig. 5 Static structure factor of (a) fully, (b) propyl partially, and (c) hydroxyl partially deuterated 2-propanol obtained by integrating the AMATERAS data in the energy domain. These structure factors contain the contribution of both the coherent and incoherent scattering (this latter being an exponentially decaying Debye Waller factor, most notable in panel c).

ATERAS of fully deuterated and partially deuterated samples of 2-propanol. Whereas in the fully deuterated sample the intensity of the pre-peak decreases, in hydroxyl and propyl partially deuterated 2-propanol the scattered intensity at ≈ 0.8 Å^{-1} increases. Interestingly, whereas at room temperature propyl deuterated 2-propanol does not show a clear pre-peak, in the glassy state, at $T = 20$ K, it does. Finally, we remark here that both the main peak and the pre-peak move to higher Q as temperature is lowered, which can be explained by an increased density; however, the ratio of the peak position changes from ≈ 0.5 to ≈ 0.6 (see Figure S3[60,60]) indicating a densification of the hydrophobic volumes separating the H-bonding associates beyond the one of the interparticle distance. In summary, as temperature is lowered the 2-propanol molecules increasingly order themselves to accommodate the sprawling H-bond network.

3.2 Dynamics

3.2.1 Quasi-elastic neutron scattering experiment

In order to investigate the effect of H-bonding and of the presence of H-bonding associates on the dynamics of 2-propanol, we carried out QENS and NSE neutron scattering measurements. The combination of multiple neutron scattering techniques allowed us to perform measurements covering a wide range of timescale from fractions of a picosecond to several nanoseconds over the relevant Q range encompassing the pre-peak and main peak.

The intermediate scattering function for 2-propanol was modeled as a combination of an exponential and a stretched exponential function as

$$\begin{aligned}\frac{I(Q,t)}{I(Q,0)} &= [1-A'(Q)]\delta(t)+A'(Q)\{[1-A(Q)]e^{-\frac{t}{\tau_s(Q)}} \\ &\quad +A(Q)e^{-\left(\frac{t}{\tau_l(Q)}\right)^{\beta(Q)}}\} \end{aligned} \quad (8)$$

where the $[1-A'(Q)]\delta(t)$ term ensures proper normalization and accounts for processes outside the experimental window, the exponential term represents a faster dynamic process corresponding to local relaxations and the stretched exponential term represents a slower process related to the molecular structural relaxation over length scales beyond the nearest neighbors. Typically, the local relaxation is attributed to the motions of carbon chains in monohydroxy alcohols and the corresponding time scale for small molecules such as 2-propanol is hundreds of femtosecond, which falls at the limit of the time window of the neutron spectrometers employed here. Therefore, in the following, we focus on the analysis of the long time stretched exponential term; at the main peak, this term is related to the structural relaxation and at the pre-peak reveals the dynamics of the mesoscale structures, *i.e.*, their diffusion and lifetime.

The fitting of the AMATERAS data was performed in the energy domain:

$$S_{\exp}(Q,E) = Amp(Q)\cdot\mathscr{F}\left\{\frac{I(Q,t)}{I(Q,0)}\right\}\otimes R(Q,E) \quad (9)$$

where $S_{\exp}(Q,E)$ represents the experimental values of the dynamic structure factor, $\mathscr{F}\{\cdots\}$ indicates a Fourier transform, $\otimes$ represents the convolution operation, $Amp(Q)$ is the spectral area, and $R(Q,E)$ is the Q-dependent instrument resolution; the Fourier transform of the $[1-A'(Q)]\delta(t)$ term yields a Q-dependent background. Two examples of the fitting results of AMATERAS data at the structure factor pre-peak (subplot (a), (b), and (c)) and main peak (subplot (d) and (e)) are shown in Figure 6. The exponential term has to be considered to obtain satisfactory fitting of the data, but the Q and T dependence of the short time dynamics cannot be extracted with accuracy because they are too fast for the energy window explored.

Figure 7 shows the Q dependence of the slower relaxation time τ_l and the stretch exponent β, at room temperature. The characteristic relaxation time τ_l shows a maximum at both the pre-peak and main peak, an occurrence which is referred to as de Gennes narrowing[82]. In correspondence with peaks in the structure factor, the collective dynamics slows down as a consequence of the enhanced cooperativity between molecules, as first observed in atomic liquids[82] but also in correspondence of the pre-peak in some alcohols[23,26]. Meanwhile, the mild peaking of the stretch exponent β at both the pre-peak and main peak, indicates a slightly more homogeneous dynamics in comparison to the other Q values. This finding can be understood considering that a narrower distribution of possible relaxation processes dominates at length scales specified by the structure factor peaks, either related to the dynamics of the H-bonded associates at the pre-peak or to the structural relaxation at the main peak. In other words, at the main peak, where Q corresponds to the distance between two 2-propanol molecules, the measured relaxation is, within certain approximations[45], principally determined by the motions of single molecules in and out of the first coordination shell, a process referred to as the structural relaxation; at the structure factor pre-peak, in contrast, the probed dynamics corresponds to the dynamics of the H-bonded associates, which is approximately an order of magnitude slower, consistent with previous observations[21]. In 1-propanol, it was shown that the timescale measured by neutron scattering at the pre-peak matches the one observed using ^{1}H and ^{2}H spin relaxation Nuclear Magnetic Resonance (NMR) spectroscopy and associated with the lifetime of the hydrogen bonding. Therefore, our neutron scattering measurements at the pre-peak are interpreted to probe the dissociation of the H-bonds associates.

As far as the temperature dependence of the dynamics at the structure factor peak is concerned, both the prefactor A and the stretching exponent β depend little on temperature. Therefore, we further fixed $A = 0.80$ and β=0.58 as the corresponding maximum likelihood values and fitted the data again with fewer degrees of freedom.

Comparing to the AMATERAS measurements at the picosecond time scale, Figure 8 shows the normalized ISFs of 2-propanol measured by NSE at temperatures covering both liquid and supercooled states. The short time dynamics, *i.e.* the exponential term in equation 8, is almost completely outside the time window probed at NSE and, therefore, the NSE data could be analyzed for $t > 50$ ps using only the second component of the ISF defined in

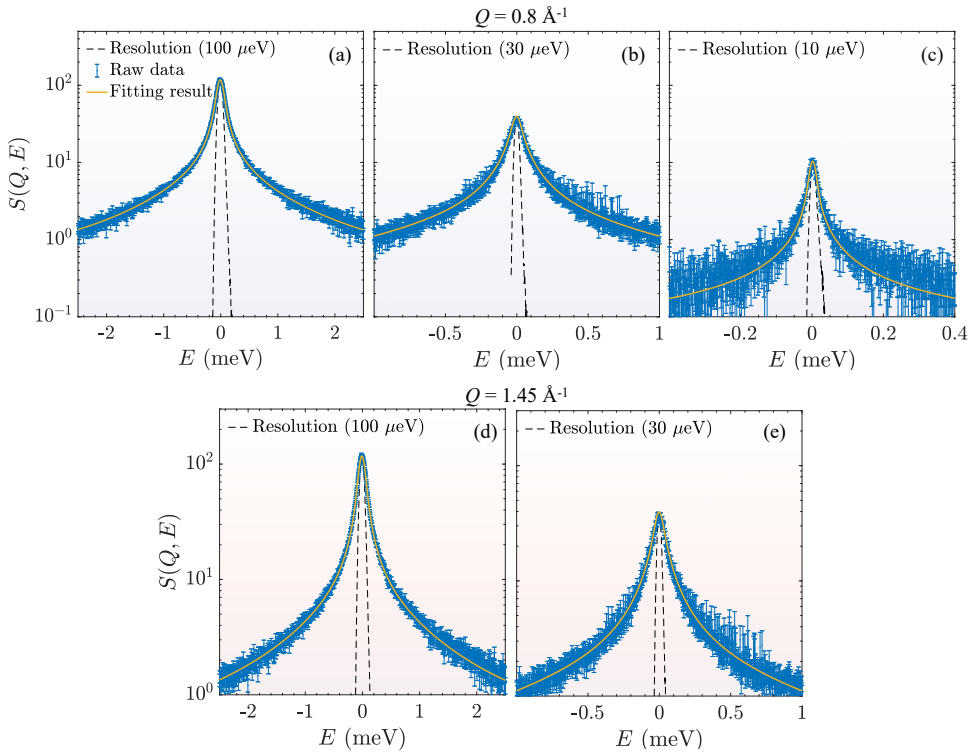

Fig. 6 Examples of the fits of the QENS measurements at AMATERAS. (a), (b), and (c) show the global fitting results using instrumental resolutions of (100, 30, and 10) μeV respectively at the structure factor pre-peak at 280 K. (d) and (e) show the global fitting results using instrumental resolutions of 100 μeV and 30 μeV respectively at the main peak at 280 K.

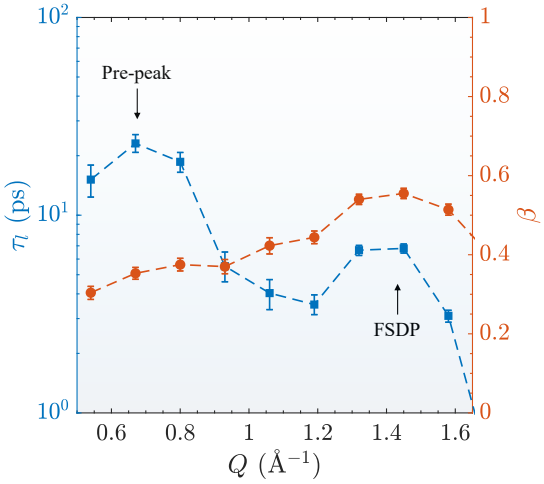

Fig. 7 Slower relaxation time τ_l and stretch exponent β as functions of Q. The de Gennes narrowing phenomenon can be clearly observed as the characteristic relaxation time increases at both the structure factor pre-peak and main peak.

Equation 8:

$$\frac{I(Q,t)}{I(Q,0)} = A''(Q)e^{-\left(\frac{t}{\tau_l(Q)}\right)^{\beta(Q)}} \tag{10}$$

where $A'' = AA'$.

After a preliminary fitting, it was observed that the amplitude, A'', and the stretching exponent, β, were temperature independent within experimental uncertainties at both the structure factor pre-peak and main peak (see Figure S5[60]). Therefore, for each Q, the data were analyzed globally at all temperatures using a common A'' and a common β value, yielding satisfactory fits (see Tables S1 and S2[60]). The validity of this *ansatz* is further supported by the possibility of creating master curve of the data at all temperatures by simply rescaling the time axis, as shown in Figure S6[60]. This analysis yields $A'' = 0.43 \pm 0.01$, $\beta = 0.65 \pm 0.02$ at the pre-peak and $A'' = 0.81 \pm 0.01$, $\beta = 0.56 \pm 0.01$ at the main peak, this latter in good agreement with the AMATERAS results. † It is remarkable that the value of A'' is noticeably smaller than 1 at the pre-peak because it indicates a significant rearrangement of the H-bonded structures through local relaxation, without, how-

† Furthermore, a global fit of the data in the whole time range at all temperatures using Equation 8, with A′, A, and β temperature independent and only τ_l and τ_s changing with T, was also performed. This alternative analysis yields results, reported in Figure S8[60], matching with the ones reported in the main text within uncertainty. The simpler fit according to Equation 10 is reported in the main text because some of the data sets lack the short time data points. For the reader reference, the obtained results are at the pre-peak A′ = 0.626 ± 0.008, A = 0.65 ± 0.01, β = 0.69 ± 0.02, and at the main peak A′ = 1.06 ± 0.07, A = 0.78 ± 0.05, β = 0.54 ± 0.02.

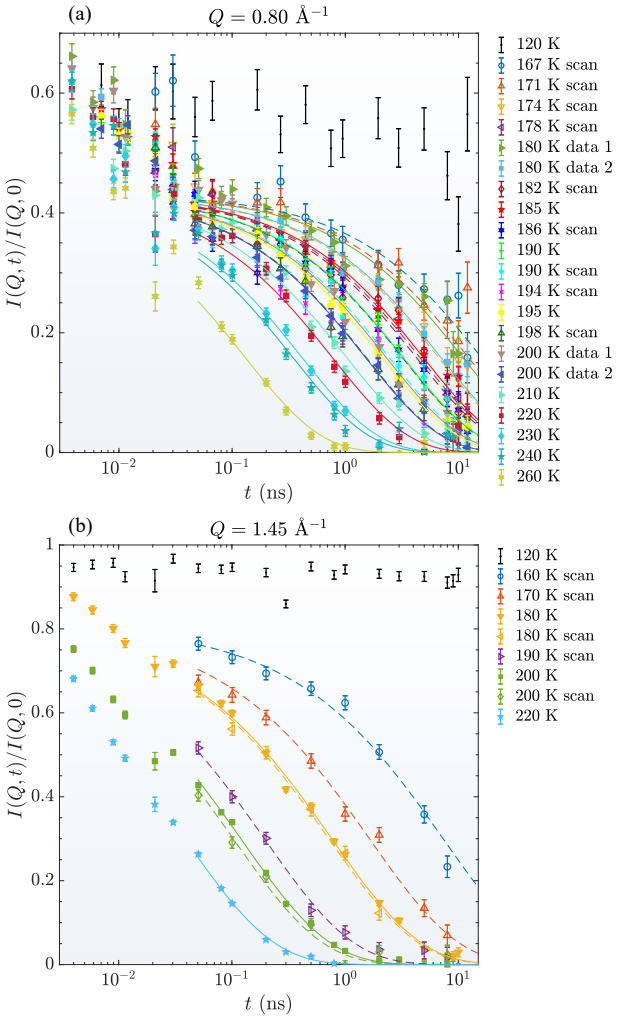

Fig. 8 Intermediate scattering functions of 2-propanol at the (a) structure factor pre-peak and (b) main peak, at various temperatures covering liquid and supercooled liquid states measured by NSE spectrometer. "scan" indicates that the corresponding measurements were performed during cooling. The solid and dash lines represent the best fit of the ISFs measured at fixed temperature and in the scanning mode using Equation 10 for $t \geq 50$ ps, respectively. The "data 1" and "data 2" in (a) indicate two independent measurements at the same temperature.

ever, fully breaking the supramolecular association.

The average relaxation time of a stretched exponential can be calculated as

$$\langle \tau_l \rangle = \int_0^\infty e^{-(\frac{t}{\tau_l})^\beta} dt = \frac{\tau_l}{\beta}\Gamma(\frac{1}{\beta}) \tag{11}$$

where $\Gamma(x)$ represents the gamma function.

The NSE results of the average relaxation time are generally in good agreement with the values obtained from the AMATERAS data; however, away from the main peak, the contribution of the incoherent scattering to the ToF data cannot be neglected (whereas on NSE, the weight of the incoherent contribution is reduced by a factor of 3 and the coherent scattering contribution is dominant). This occurrence prevents the use of the AMATERAS data to probe the dynamics of the pre-peak as temperature is decreased.

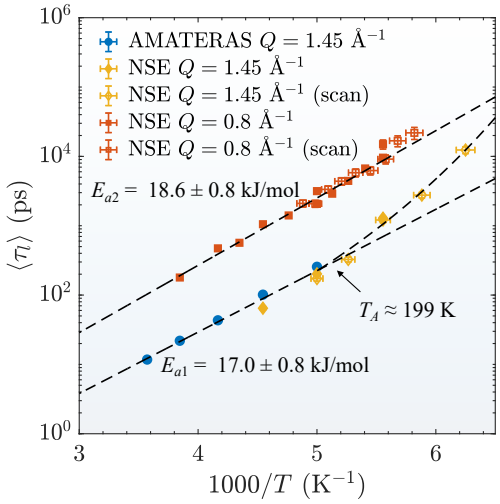

Fig. 9 Average relaxation time measured by QENS measurements at temperature ranging from liquid state to supercooled liquid state. The fits of the QENS data at the main peak and the non-scan data at the pre-peak are shown as the dash lines. Data at the pre-peak measured using scan mode are shifted to the fitting curve by imposing consistency with the measurements measured at a stationary temperature as detailed in Figure S7[60].

The comparison between the average relaxation times measured at the pre-peak and main peak is shown in Figure 9, as a function of temperature. At the main peak, we observe a super Arrhenius behavior, with an Arrhenius crossover temperature $T_A \approx 199$ K below which the temperature dependence of the relaxation time starts to deviate from the Arrhenius relation. The crossover indicates the emergence of cooperativity and dynamical heterogeneity[83,84]. The relaxation process at the main peak, as discussed above, is related with the structural relaxation. At high temperature, free diffusion predominates the dynamics, which is characterized by an Arrhenius dependence of the transport properties. As the temperature decreases below T_A, the cage formed by the nearest neighbors can endure hundreds of vibrational periods without breaking. In this way, the dynamic heterogeneity generated by the uneven local environments manifests

as a non-Arrhenius temperature dependence of transport properties. By fitting the relaxation time within the temperature range above T_A, we can obtain the corresponding activation energy as $E_{a1} = (17.0 \pm 0.8)$ kJ/mol.

In contrast, the relaxation time at the structure factor pre-peak, where the dynamics is dominated by the disassociation and re-formation of the supramolecular clusters, exhibits an Arrhenius temperature dependence in the whole temperature range probed in our experiments, down to 173 K, which corresponds to $T/T_m \approx 0.94$. The activation energy is measured, using only the measurements performed at temperature equilibrium (no scan) to be $E_{a2} = (18.6 \pm 0.8)$ kJ/mol, which is larger than the activation energy at the main peak and approximates the activation energy of the viscosity as $E_\eta = (21.2 \pm 0.1)$ kJ/mol (see Figure S9[60]). ‡ This demonstrates the relevance of H-bonded associates in determining the transport properties of 2-propanol. In fact, the Kubo-Green theory states that the steady-state shear viscosity of liquids is given by the time correlation function of shear stress which, within the site-site Mode Coupling Theory (MCT), can be approximated by the partial intermediate scattering function. Thus, it has been shown that the dynamics at the pre-peak affects the viscosity of a liquid. The contribution of mesoscale structure to the viscosity was observed in the case of methanol[24] and dodecanol[26], without any investigation of its temperature dependence. It is noteworthy, therefore, that in 2-propanol the dynamics of the H-bonded associates approximates the temperature dependence of the transport properties.

As far as the glassy behavior of 2-propanol is concerned, in the liquid state, the viscosity of 2-propanol follows an Arrhenius behavior, however, an Angell plot (see Figure S9[60]) clearly indicates that it is a rather fragile liquid and that a markedly non-Arrhenius behavior appears in the supercooled state. As temperature is lowered, the structural relaxation observed at the main peak deviates from the Arrhenius behavior approaching the timescale of the associates as probed at the pre-peak. As the dynamic cooperativity sets in, the distinction between the dynamics of the H-bonded associates and of the individual molecules tends to vanish.

As mentioned in the introduction, monohydroxy alcohols exhibit a rich dynamic landscape with multiple relaxation processes. The average relaxation times obtained by our investigation using neutron scattering can be compared with the results of dielectric spectroscopy measurements by Murthy and Nayak[15] and by Sato and Buchner[85], as shown in Figure S10[60]. At room temperature at least four relaxation processes have been identified by Dielectric Relaxation (DR) spectroscopy. The dynamics at the main peak is slightly faster but has a similar time scale to the γ process identified by Murthy and Nayak[15] and τ_2 relaxation time reported by Sato and Buchner[85]. The dynamics of the H-bonded associates probed at the pre-peak by neutron scattering has similar time scale to the α_2 process identified by Murthy and Nayak[15] and τ_1 relaxation time reported by Sato and Buchner.[85] Thus, the neutron scattering results indicate the microscopic origin of these dynamic processes observed by DR and provides indication of their temperature dependence, which had not been reported in the temperature between $\approx$ 270 K and $\approx$ 145 K. The emerging picture is consistent with the Transient Chain Model (TCM)[32] which describes three possible relaxation mechanisms for chain forming H-bonding alcohols: i) the acyl chain dynamics, in most cases coinciding with the α relaxation; ii) the breaking of H-bonding associates, at intermediate time scales, which can be probed by Nuclear Magnetic Relaxation (NMR) techniques; iii) and the re-orientation of the H-bonding associates, which is at the origin of the Debye relaxation process in alcohols. Within this scenario, neutron scattering studies on 1-propanol[21] and methanol[22,23] indicate that the structural relaxation observed at the main peak matches the α relaxation observed with DR, whereas the dynamics at the pre-peak is associated to the breaking and formation of the H-bonding associates.

However, a noteworthy variation, not previously observed, is the difference in the temperature dependence of the associate dynamics from the structural relaxation. Previous spectroscopic results on 1-propanol[21,86] and n-butanol[32] indicate a similar temperature dependence of the structural relaxation and the associates' dynamics. In fact, within the TCM the associates dynamics has the same time scale as the structural relaxation multiplied by the number of molecules in the associates.[32] The present data differ from this behavior; whereas our simulations indicate an increase of the number of associated molecules as the temperature decreases, the NSE data show that the timescales of the dynamics at the pre-peak and the main peak approach each other as temperature is lowered. Such behavior is attributed to the structural coupling between the hydrophobic and H-bonded domains as temperature is lowered; in fact, as discussed above, Figure 5 demonstrates an increasing negative correlation between the propyl and hydroxyl group as well as an increased structuring across propyl groups with decreasing temperature. The origin of the difference with the behavior reported for 1-propanol[21] and n-butanol[32] could be due to the difference in the dynamics probed by neutron scattering and NMR techniques, which could manifest itself in the supercooled temperature region. Alternatively, the differing behavior could be due to the presence of ring and tree like structures in 2-propanol. Further investigation of other mono-hydroxy alcohols in the supercooled region using various spectroscopy techniques, including neutron scattering, would be needed to address this question.

It is noteworthy that, around the glass transition temperature at $T = 120$ K, the measured normalized ISF at the pre-peak takes a time independent value of ≈ 0.6 (whereas at the main peak approximates unity), indicating the presence of fast relaxation processes outside the measured window. The long time relaxation process measured at the pre-peak was characterized by an amplitude of $A'' = 0.43$, which indicates that the fast relaxation process (whose tail is observed at short times in the NSE measurements) has an amplitude of ≈ 0.2; this process becomes too slow to be clearly observed in the NSE time window at 120 K. Whether, at temperatures below the ones investigated here, the

‡ It would be interesting at this point to compare our results with the Maxwell time, $\tau_{Maxwell} = \eta/G_\infty$, G_∞ being the high-frequency shear modulus. However, to the best of our knowledge, G_∞ has not been determined for 2-propanol. To provide the reader with a point of reference, we report $\tau_{Maxwell} \approx 94$ ps at 228 K using the G_∞ value for 1-propanol[43].

dynamics at the pre-peak transitions to a super-Arrhenius behavior and whether a merging of different relaxation processes takes place are interesting open question. These points could be investigated by extending the temperature and time range, but that is infeasible with current instrument capabilities.

3.2.2 Molecular dynamics simulation

As a complement to the neutron scattering measurements, MD simulations can provide further microscopic insights on both the local structure relaxation and the dynamics of the supramolecular clusters.

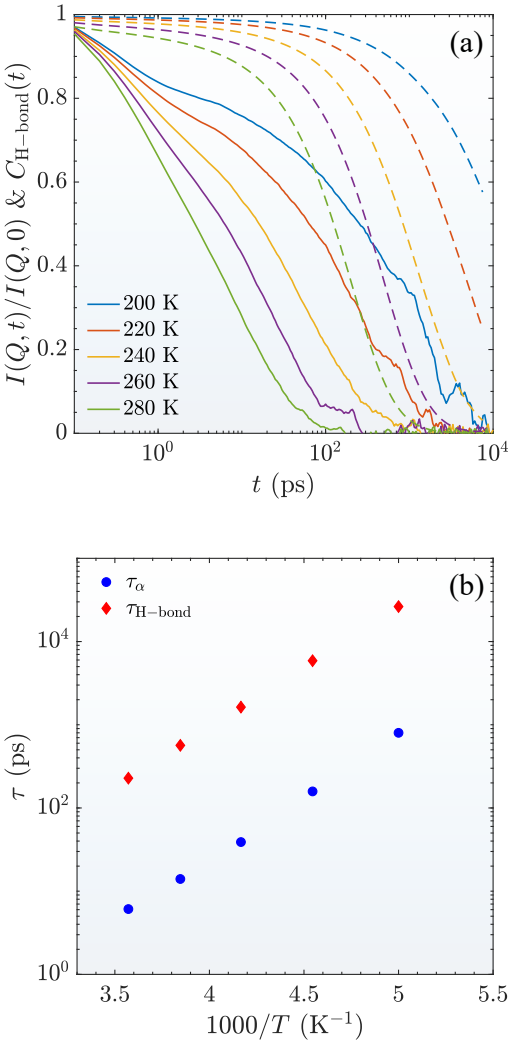

Fig. 10 (a) Collective intermediate scattering function at the main peak (solid lines) and hydrogen bond autocorrelation function (dash lines) of 2-propanol from 200 K to 280 K calculated from MD simulations. (b) Local structural relaxation times (blue dots) as the collective intermediate scattering function decays to $1/e$, and, average relaxation time of supramolecular clusters (red diamonds) obtained by fitting the slower segments hydrogen bond autocorrelation functions with a stretched exponential function and using Equation 11, as functions of inverse temperature.

The local structural relaxation in simulations can be characterized by the collective ISF at the main peak as the solid lines in Figure 10(a) demonstrates. Although the MD simulation does not match the QENS measurements quantitatively due to the utilization of a generic force field, the collective ISFs clearly show a similar two-step decay process corresponding to the relaxation model used to analyze the experimental data above. To characterize the dynamics of the H-bonded associates, we also calculated the hydrogen bond aurocorrelation function shown as the dash lines in Figure 10(a) defined as[87]

$$C_{\mathrm{H-bond}}(t) = \left\langle \frac{\sum_{i,j=1}^{N} h_{i,j}(0)h_{i,j}(t)}{\sum_{i,j=1}^{N} h_{i,j}^2(0)} \right\rangle \tag{12}$$

where N is the total number of molecules in the system and the Boolean function $h_{i,j}(t)$ indicates the existence of hydrogen bond between molecules, which, is equal to 1 if the i-th and j-th molecules form a hydrogen bond at time t and equal to 0 otherwise.

The decay of the hydrogen bond autocorrelation function is obviously much slower than the corresponding ISF, indicating a decoupling between the local structural relaxation and the involvement of the supramolecular clusters. In fact, the characteristic relaxation time of the supramolecular clusters can be directly compared with the local structural relaxation time. We extracted the local structural relaxation time as the time needed for $I(Q,t)$ at the main peak to decay to $1/e$.[57] The average relaxation time of supramolecular clusters was obtained by fitting the slower segments of the hydrogen bond autocorrelation functions with a stretched exponential function. As Figure 10(b) shows, the relaxation time of the clusters largely exceeds the local structural relaxation time. Since the local structural relaxation does not necessarily involve the breaks of hydrogen bonds, one cluster can diffuse, rotate, and deform which only contributes to the structural relaxation. However, as temperature lowers, i) the density increases as indicated by the shift towards higher Q values of both the pre-peak and the main peak, and, ii) the H-bond network becomes more and more persistent due to the increased number of large clusters, which results in a stronger coupling between the hydrophobic and H-bonded domains. These observations are put in evidence by the strengthening of the feature observed in correspondence of the Q value of the pre-peak in the cross-term of the partial structure factor (between the hydroxyl groups and the remaining of the 2-propanol molecule). A consistent explanation is that the structural relaxation increasingly happens only if it is facilitated by a breaking of the H-bond network.

4 Conclusions

In this work, using combined QENS and NSE neutron scattering techniques and the support of MD simulations, we have investigated the molecular dynamics of a model H-bonding liquid 2-propanol. The combined measurements and simulations of a series of samples differing for their deuteration scheme has brought to light how as temperature is lowered an increasing structuring of the hydrophobic domains around the sprawling H-bond network takes place. The structural relaxation and the dynamics of the H-bonding associates was investigated experimentally measuring the relaxation time at the main peak and at the pre-

peak. The formation and disgregation of the H-bond associates is a process slower than the structural relaxation, which affects the temperature dependence of the viscosity. Such process remains Arrhenius even (at least just) below the melting temperature in the supercooled state. On the other hand, the structural relaxation measured at the main peak shows a super-Arrhenius temperature dependence already in the liquid state on approaching the melting temperature. We speculate that the increased structural coupling between the hydrophobic and H-bonded domains originates the acceleration in the slowing down of the dynamics as temperature is lowered. These results highlight how different structures, over different length scales, might play a more or less relevant role at various temperatures in determining the behavior of an amorphous system.

Associated Content

Supplementary Information: Comparison between simulated and experimental 2-propanol density; Size distributions of the supramolecular clusters from 50 to 1000; temperature dependence of the structure factor of deuterated 2-propanol; temperature dependence of the structure factor of deuterated 1-propanol; fitting results for the fitting of the NSE data individually at each temperature; fitting results for the analysis of the NSE data; master curve of the NSE data at different temperatures; Arrhenius plot of the relaxation time using the nominal sample temperature; global fitting results for the NSE data using Equation 8; Angell plot of the dynamic viscosity of deuterated 2-propanol; relaxation map for 2-propanol including the present neutron results and previous dielectric measurements [15,85].

Disclaimer

The identification of any commercial product or trade name does not imply endorsement or recommendation by the National Institute of Standards and Technology. Uncertainties and error bars throughout this letter represent the confidence interval of one standard deviation.

Conflicts of interest

There are no conflicts to declare.

Acknowledgements

This material is based upon work supported by the U.S. Department of Energy, Office of Science, Office of Basic Energy Sciences, Materials Sciences and Engineering Division, under Award Number DE-SC0014084. Access to the NGA NSE Instrument was provided by the Center for High Resolution Neutron Scattering, a partnership between the National Institute of Standards and Technology and the National Science Foundation under Agreement No. DMR-1508249. AMATERAS experiment was performed with approval of J-PARC Center (Proposal number: 2012A0046 and 2014B0262). MN acknowledges funding support of cooperative agreement No. 70NANB15H259 from the National Institute of Standards and Technology, U.S. Department of Commerce.

Notes and references

1 F. H. Stillinger, *Science*, 1980, **209**, 451–457.
2 A. Luzar and D. Chandler, *Nature*, 1996, **379**, 55.
3 G. A. Jeffrey, *An introduction to hydrogen bonding*, Oxford University Press, 1997.
4 J. R. Errington and P. G. Debenedetti, *Nature*, 2001, **409**, 318.
5 P. L. Geissler, C. Dellago, D. Chandler, J. Hutter and M. Parrinello, *Science*, 2001, **291**, 2121–2124.
6 Y. Zhang, A. Faraone, W. A. Kamitakahara, K.-H. Liu, C.-Y. Mou, J. B. Leão, S. Chang and S.-H. Chen, *Proceedings of the National Academy of Sciences*, 2011, **108**, 12206–12211.
7 J. D. Watson and F. H. C. Crick, *Nature*, 1953, **171**, 737–738.
8 J. D. Watson and F. H. C. Crick, *Nature*, 1953, **171**, 964–967.
9 E. N. Nikolova, H. Zhou, F. L. Gottardo, H. S. Alvey, I. J. Kimsey and H. M. Al-Hashimi, *Biopolymers*, 2013, **99**, 955–968.
10 L. Pauling, R. B. Corey and H. R. Branson, *Proceedings of the National Academy of Sciences*, 1951, **37**, 205–211.
11 A. Ben-Naim, *The Journal of Physical Chemistry*, 1991, **95**, 1437–1444.
12 G. D. Rose and R. Wolfenden, *Annual review of biophysics and biomolecular structure*, 1993, **22**, 381–415.
13 M. Tarek and D. J. Tobias, *Physical Review Letters*, 2002, **88**, 138101.
14 P. Zetterström, U. Dahlborg, R. G. Delaplane and W. S. Howells, *Physica Scripta*, 1991, **44**, 56.
15 S. S. N. Murthy and S. K. Nayak, *The Journal of Chemical Physics*, 1993, **99**, 5362–5368.
16 L.-M. Wang and R. Richert, *The Journal of Physical Chemistry B*, 2005, **109**, 8767–8773.
17 A. Sahoo, S. Sarkar, P. S. R. Krishna, V. Bhagat and R. N. Joarder, *Pramana*, 2008, **71**, 133–141.
18 A. Sahoo, S. Sarkar, P. S. R. Krishna and R. N. Joarder, *Pramana*, 2010, **74**, 765–779.
19 C. Gainaru, S. Kastner, F. Mayr, P. Lunkenheimer, S. Schildmann, H. J. Weber, W. Hiller, A. Loidl and R. Böhmer, *Physical Review Letters*, 2011, **107**, 118304.
20 S. Bauer, K. Burlafinger, C. Gainaru, P. Lunkenheimer, W. Hiller, A. Loidl and R. Böhmer, *The Journal of Chemical Physics*, 2013, **138**, 094505.
21 P. Sillrén, A. Matic, M. Karlsson, M. Koza, M. Maccarini, P. Fouquet, M. Götz, T. Bauer, R. Gulich, P. Lunkenheimer, A. Loidl, J. Mattsson, C. Gainaru, E. Vynokur, S. Schildmann, S. Bauer and R. Böhmer, *The Journal of Chemical Physics*, 2014, **140**, 124501.
22 C. E. Bertrand, J. L. Self, J. R. D. Copley and A. Faraone, *The Journal of Chemical Physics*, 2016, **145**, 014502.
23 C. E. Bertrand, J. L. Self, J. R. D. Copley and A. Faraone, *The Journal of Chemical Physics*, 2017, **146**, 194501.
24 T. Yamaguchi and A. Faraone, *The Journal of Chemical Physics*, 2017, **146**, 244506.
25 W. Chen, S. Watson, Y. Qiu, J. A. Rodriguez-Rivera and A. Faraone, *Physica B: Condensed Matter*, 2019, **564**, 166–171.
26 T. Yamaguchi, A. Faraone and M. Nagao, *The Journal of Physical Chemistry B*, 2019, **123**, 239–246.

27 M. Wilson and P. A. Madden, *Physical Review Letters*, 1994, **72**, 3033.

28 T. Kosztolányi, I. Bakó and G. Pálinkás, *The Journal of Chemical Physics*, 2003, **118**, 4546–4555.

29 M. Paolantoni, P. Sassi, A. Morresi and R. S. Cataliotti, *Chemical Physics*, 2005, **310**, 169–178.

30 F. Palombo, P. Sassi, M. Paolantoni, A. Morresi and R. S. Cataliotti, *The Journal of Physical Chemistry B*, 2006, **110**, 18017–18025.

31 P. Sillrén, J. Bielecki, J. Mattsson, L. Börjesson and A. Matic, *The Journal of Chemical Physics*, 2012, **136**, 094514.

32 C. Gainaru, R. Meier, S. Schildmann, C. Lederle, W. Hiller, E. A. Rössler and R. Böhmer, *Physical Review Letters*, 2010, **105**, 258303.

33 P. Sillrén, J. Swenson, J. Mattsson, D. Bowron and A. Matic, *The Journal of Chemical Physics*, 2013, **138**, 214501.

34 S. W. Benson, *Journal of the American Chemical Society*, 1996, **118**, 10645–10649.

35 R. Ludwig, *ChemPhysChem*, 2005, **6**, 1369–1375.

36 A. Sahoo, S. Sarkar, V. Bhagat and R. N. Joarder, *The Journal of Physical Chemistry A*, 2009, **113**, 5160–5162.

37 W. Dannhauser, *The Journal of Chemical Physics*, 1968, **48**, 1911–1917.

38 L. P. Singh, C. Alba-Simionesco and R. Richert, *The Journal of Chemical Physics*, 2013, **139**, 144503.

39 L. P. Singh and R. Richert, *Physical Review Letters*, 2012, **109**, 167802.

40 W. Dannhauser and R. H. Cole, *The Journal of Chemical Physics*, 1955, **23**, 1762–1766.

41 M. A. Floriano and C. A. Angell, *The Journal of Chemical Physics*, 1989, **91**, 2537–2543.

42 J. Barthel, K. Bachhuber, R. Buchner and H. Hetzenauer, *Chemical Physics Letters*, 1990, **165**, 369–373.

43 R. Kono, T. A. Litovitz and G. E. McDuffie, *The Journal of Chemical Physics*, 1966, **45**, 1790–1796.

44 T. Iwashita, D. M. Nicholson and T. Egami, *Physical Review Letters*, 2013, **110**, 5.

45 B. Wu, T. Iwashita and T. Egami, *Physical Review Letters*, 2018, **120**, 6.

46 P. Debye, *Ver. Deut. Phys. Gesell.*, 1913, **15**, 777–793.

47 D. Xu, S. Feng, J.-Q. Wang, L.-M. Wang and R. Richert, *Journal of Physical Chemistry Letters*, 2020, **11**, 5792–5797.

48 M. Paluch, C. M. Roland, S. Pawlus, J. Zioło and K. L. Ngai, *Physical Review Letters*, 2003, **91**, 115701.

49 Y. H. Liu, T. Fujita, D. P. B. Aji, M. Matsuura and M. W. Chen, *Nature Communications*, 2014, **5**, 1–7.

50 M. Bee, *Quasielastic neutron scattering*, 1988.

51 F. Mezei, *Neutron spin echo lecture notes in physics*, 1980.

52 H. Tanaka, T. Kawasaki, H. Shintani and K. Watanabe, *Nature Materials*, 2010, **9**, 324–331.

53 S. Marín-Aguilar, H. H. Wensink, G. Foffi and F. Smallenburg, *Physical Review Letter*, 2020, **124**, 208005.

54 A. Sanz, M. Jiménez-Ruiz, A. Nogales, D. M. y Marero and T. A. Ezquerra, *Physical Review Letters*, 2004, **93**, 015503.

55 J. S. Gardner, G. Ehlers, A. Faraone and V. Garcia-Sakai, *Nature Review Physics*, 2020, **2**, 103–116.

56 G. L. Squires, *Introduction to the theory of thermal neutron scattering*, Cambridge University Press, 1978.

57 J.-P. Hansen and I. R. McDonald, *Theory of simple liquids*, Elsevier, 1990.

58 N. Rosov, S. Rathgeber and M. Monkenbusch, *ACS Symposium Series*, 2000, **739**, 103–116.

59 A. M. Gaspar, S. Busch, M.-S. Appavou, W. Haeussler, R. Georgii, Y. Su and W. Doster, *Biochimica et Biophysica Acta (BBA)-Proteins and Proteomics*, 2010, **1804**, 76–82.

60 Supplemental Information.

61 K. Nakajima, S. Ohira-Kawamura, T. Kikuchi, M. Nakamura, R. Kajimoto, Y. Inamura, N. Takahashi, K. Aizawa, K. Suzuya, K. Shibata, T. Nakatani, K. Soyama, R. Maruyama, H. Tanaka, W. Kambara, T. Iwahashi, Y. Itoh, T. Osakabe, S. Wakimoto, K. Kakurai, F. Maekawa, M. Harada, K. Oikawa, R. E. Lechner, F. Mezei and M. Arai, *Journal of the Physical Society of Japan*, 2011, **80**, SB028.

62 R. T. Azuah, L. R. Kneller, Y. Qiu, P. L. W. Tregenna-Piggott, C. M. Brown, J. R. D. Copley and R. M. Dimeo, *Journal of Research of the National Institute of Standards and Technology*, 2009, **114**, 341–358.

63 M. Nakamura, R. Kajimoto, Y. Inamura, F. Mizuno, M. Fujita, T. Yokoo and M. Arai, *Journal of the Physical Society of Japan*, 2009, **78**, 093002–093002.

64 Y. Inamura, T. Nakatani, J. Suzuki and T. Otomo, *Journal of the Physical Society of Japan*, 2013, **82**, SA031.

65 P. Kienzle, *Bumps: Curve fitting and uncertainty analysis*, 2018.

66 J. A. Vrugt, J. M. Hyman, B. A. Robinson, D. Higdon, C. J. F. Ter Braak and C. G. H. Diks, *Accelerating Markov chain Monte Carlo simulation by differential evolution with self-adaptive randomized subspace sampling*, Los Alamos National Lab.(LANL), Los Alamos, NM (United States) Technical Report 3, 2008.

67 MATLAB, *version 9.4.0 (R2018a)*, The MathWorks Inc., Natick, Massachusetts, 2018.

68 H. J. C. Berendsen, D. van der Spoel and R. van Drunen, *Computer Physics Communications*, 1995, **91**, 43–56.

69 W. L. Jorgensen and J. Tirado-Rives, *Journal of the American Chemical Society*, 1988, **110**, 1657–1666.

70 B. Hess, H. Bekker, H. J. C. Berendsen and J. G. E. M. Fraaije, *Journal of Computational Chemistry*, 1997, **18**, 1463–1472.

71 U. Essmann, L. Perera, M. L. Berkowitz, T. Darden, H. Lee and L. G. Pedersen, *The Journal of Chemical Physics*, 1995, **103**, 8577–8593.

72 S. Nosé, *The Journal of Chemical Physics*, 1984, **81**, 511–519.

73 S. Nosé, *Molecular Physics*, 1984, **52**, 255–268.

74 W. G. Hoover, *Physical Review A*, 1985, **31**, 1695–1697.

75 M. Parrinello and A. Rahman, *Physical Review Letters*, 1980, **45**, 1196.

76 M. Parrinello and A. Rahman, *Journal of Applied Physics*, 1981, **52**, 7182–7190.

77 N. P. Walter, A. Jaiswal, Z. Cai and Y. Zhang, *Computer Physics Communications*, 2018, **228**, 209–218.
78 G. W. Stewart and R. M. Morrow, *Physical Review*, 1927, **30**, 232.
79 A. Ghoufi, *The Journal of Physical Chemistry B*, 2020, **124**, 11501–11509.
80 M. Haughney, M. Ferrario and I. R. McDonald, *The Journal of Physical Chemistry*, 1987, **91**, 4934–4940.
81 J. Lehtola, M. Hakala and K. Hamalainen, *The Journal of Physical Chemistry B*, 2010, **114**, 6426–6436.
82 P. G. De Gennes, *Physica*, 1959, **25**, 825–839.
83 A. Jaiswal, T. Egami, K. F. Kelton, K. S. Schweizer and Y. Zhang, *Physical Review Letters*, 2016, **117**, 205701.
84 A. Jaiswal, T. Egami and Y. Zhang, *Physical Review B*, 2015, **91**, 134204.
85 T. Sato and R. Buchner, *The Journal of Chemical Physics*, 2003, **118**, 4606–4613.
86 M. Poeschl and H. G. Hertz, *The Journal of Physical Chemistry*, 1994, **98**, 8195–8208.
87 R. J. Gowers and P. Carbone, *The Journal of Chemical Physics*, 2015, **142**, 224907.